MACRO- AND MICRO-SIMULATIONS FOR A SUBLIMATION GROWTH OF SIC SINGLE CRYSTALS.

JÜRGEN GEISER * AND STEPHAN IRLE †

Abstract. The numerous technical applications in electronic and optoelectronic devices, such as lasers, diodes, and sensors demand high-quality silicon carbide (SiC) bulk single crystal for industrial applications. We consider a SiC crystal growth process by physical vapor transport (PVT), called modified Lely method. We deal with a model for the micro and macro-scale of the sublimation processes within the growth apparatus. The macroscopic model is based on the heat equation with heat sources due to induction heating and nonlocal interface conditions, representing the heat transfer by radiation. The microscopic model is based on the quantum chemical potential and is computed with molecular dynamics. We study of the temperature evolution in the apparatus and reflect the growth behavior of the microscopic model. We present results of some numerical simulations of the micro- and macro-model of our growth apparatus.

Keywords: numerical methods, heat equation, radiation, crystal growth process, MD (molecular dynamics).
AMS subject classifications. 35K25, 35K20, 74S10, 74A25.

1. Introduction. The motivation for this study comes from the technical demand to simulate a crystal growth apparatus for SiC single crystals. The single crystals are used as a high-valued and expensive material for optoelectronics and electronics, cf. [10]. The silicon carbide (SiC) bulk single crystal are produced by a growth process through physical vapor transport (PVT), called modified Lely-method. The modeling for the thermal processes within the growth apparatus is done in [6] and [12]. In this paper, we propose one step more in the modeling the macro-scopic and microscopic parts. The idea is to exchange results from the macroscopic to the microscopic scale to obtain a feedback to the control the growth process of the SiC bulk.

2. Macroscopic model: Heat-Flux. In the following we discuss the macroscopic model, which is based on continuum equations for the heat-flux.

2.1. Mathematical Model. The underlying equations of the model are given as follows:

a.) In this work, we assume that the temperature evolution inside the gas region $\Omega_{\rm g}$ can be approximated by considering the gas as pure argon. The reduced heat equation is

$$\rho_{\rm g}\partial_t U_{\rm g} \; - \; \nabla\cdot(\kappa_{\rm g}\nabla T) = 0, \tag{2.1}$$

$$U_{\rm g} = z_{\rm Ar}\, R_{\rm Ar}\, T, \tag{2.2}$$

where T is the temperature, t is the time, and $U_{\rm g}$ is the internal energy of the argon gas. The parameters are given as $\rho_{\rm g}$ being the density of the argon gas, $\kappa_{\rm g}$ being the thermal conductivity, $z_{\rm Ar}$ being the configuration number, and $R_{\rm Ar}$ being the gas constant for argon.

*Humboldt University of Berlin, Unter den Linden 6, D-10099 Berlin, Germany, E-mail: geiser@mathematik.hu-berlin.de
†Nagoya University, Furo-cho, Chikusa-ku, Nagoya 464-8602, Japan, E-mail: sirle@iar.nagoya-u.ac.jp

b.) The temperature evolution inside the region of solid materials Ω_s, e.g. inside the silicon carbide crystal, silicon carbide powder, graphite, and graphite insulation, is described by the heat equation

$$\rho_s \, \partial_t U_s \; - \; \nabla \cdot (\kappa_s \nabla T) = f, \tag{2.3}$$

$$U_s = \int_0^T c_s(S) \, dS, \tag{2.4}$$

where ρ_s is the density of the solid material, U_s is the internal energy, κ_s is the thermal conductivity, and c_s is the specific heat.

The equations hold in the domains of the respective materials and are coupled by interface conditions, e.g. requiring the continuity for the temperature and for the normal components of the heat flux on the interfaces between opaque solid materials. On the boundary of the gas domain, i.e. on the interface between the solid material and the gas domain, we consider the interface condition

$$\kappa_g \, \nabla T \cdot \mathbf{n}_g + R - J = \kappa_s \, \nabla T \cdot \mathbf{n}_g, \tag{2.5}$$

where $\mathbf{n}_g$ is the normal vector of the gas domain, R is the radiosity, and J is the irradiosity. The irradiosity is determined by integrating R along the whole boundary of the gas domain, cf. [9]. Moreover, we have

$$R = E + J_{\text{ref}}, \tag{2.6}$$

$$E = \sigma \, \epsilon \, T^4 \quad \text{(Stefan-Boltzmann equation)}, \tag{2.7}$$

$$J_{\text{ref}} = (1 - \epsilon) \, J, \tag{2.8}$$

where E is the radiation, J_{ref} is the reflexed radiation, ϵ is the emissivity, and σ is the Boltzmann radiation constant.

The density of the heat source induced by the induction heating is determined by solving Maxwell's equations. We deal with these equations under the simplifying assumption of an axisymmetric geometry, axisymmetric electromagnetic fields, and a sinusoidal time dependence of the involved electromagnetic quantities, following [14]. The considered system and its derivation can be found in [6], [8], and [12].

In this paper, we focus on the discretization and material properties, which are important for realistic simulations. Our underlying software tool WIAS-HiTNIHS, cf. [12], allows us flexibility in the grid generation and for the material parameters.

In the next section, we describe the used discretization.

2.2. Discretization. For the discretization of the heat equation (diffusion equation), we apply the implicit Euler method in time and the finite volume method for the space discretization, cf. [3], [6], and [12]. We consider a partition $\mathcal{T} = (\omega_i)_{i \in I}$ of Ω such that, for $m \in \{s, g\}$ (with s solid, g gas) and $i \in I$, $\omega_{m,i} := \omega_i \cap \Omega_m$ defines either a void subset or a non-void, connected, and open polyhedral subset of Ω. By integrating the corresponding heat equation (2.1) or (2.3) over $\omega_{m,i}$, we derive the following nonlinear equations for the temperature variables,

$$\begin{aligned} &\rho_m \int_{\omega_{m,i}} (U_m(T^{n+1}) - U_m(T^n)) \, r \, dx \\ &\quad - \Delta t^{n+1} \int_{\partial \omega_{m,i}} \kappa_m(T^{n+1}) \, \nabla T^{n+1} \cdot \mathbf{n}_{\omega_{m,i}} \, r \, ds \; = \; \Delta t^{n+1} \int_{\omega_{m,i}} f_m \, r \, dx, \end{aligned} \tag{2.9}$$

where the time interval is $\Delta t^{n+1} = t^{n+1} - t^n$. The temperature is given as $T^{n+1} = T(t^{n+1}, x)$, where x represents cylindrical coordinates. For the right-hand sides, we demand $f_s := f \geq 0$ and $f_g = 0$.
More details of the discretization and of dealing with the interface conditions are presented in [5], [6], [7], and [12].

In the next section, the properties of the materials in the crystal growth apparatus are described.

2.3. Material properties. For the technical realization of the apparatus, we implement the axisymmetric geometry given in [13], which is presented in Fig. 2.1. Furthermore, the properties of the materials are specified in [5], [6], and [11].

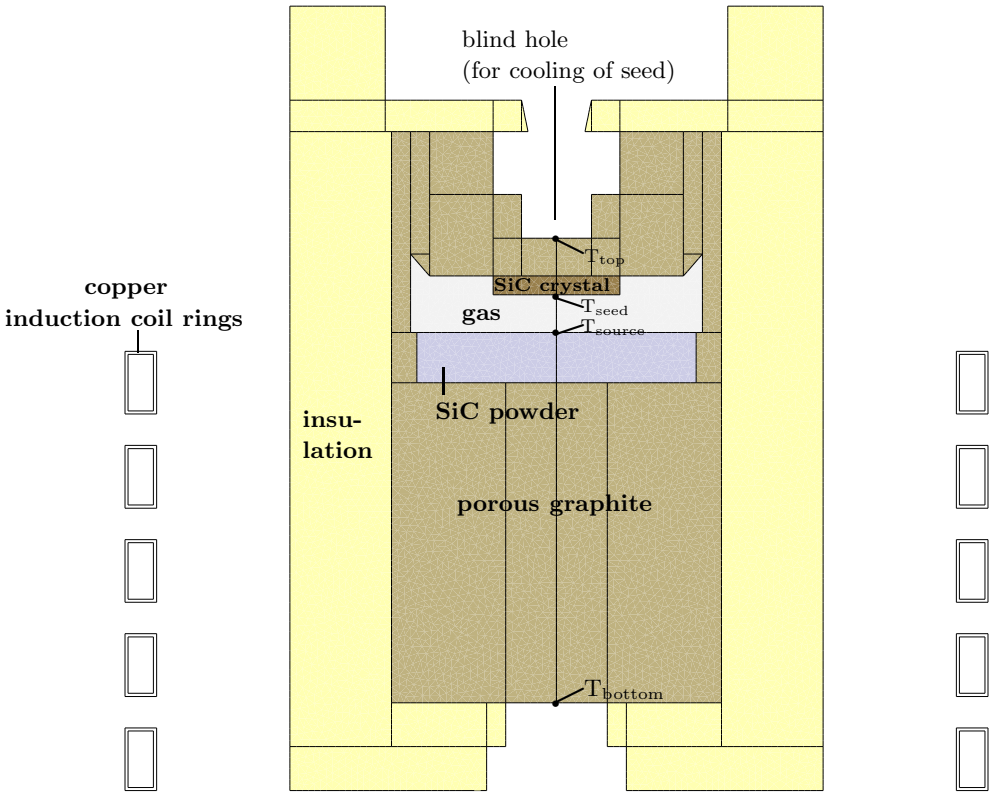

FIG. 2.1. *The growth apparatus' dimensions:* $r_{min} = 0$, $r_{max} = 8.4$ cm, $z_{min} = 0$, $z_{max} = 25.0$ cm, *the coil rings' dimensions:* $r_{min} = 4.2$ cm, $r_{max} = 5.2$ cm, $z_{min} = 0$, $z_{max} = 14.0$ cm.

Within the following specific material functions and parameters for the processes, the thermal conductivity κ is given in W/(m K), the electrical conductivity σ_c is given in 1/(Ohm m), the mass density ρ is given in kg/m^3, the specific heat c_{sp} is given in J/(K kg), the temperature T is given in K and the relative gas constant R_{Ar} is given in J/(K kg). Further the emissivity ϵ and relative magnetic permeability μ are given dimensionless.

For the gas phase (argon), we have

$$\kappa_{\mathrm{Ar}}(T) = \begin{cases} 1.83914\,10^{-4}\,T^{0.800404} & T \le 500, \\ -7.128738 + 6.610288\,10^{-2}\,T - 2.440839\,10^{-4}\,T^2 & \\ +4.497633\,10^{-7}\,T^3 - 4.132517\,10^{-10}\,T^4 + 1.514463\,10^{-13}\,T^5 & 500 \le T \le 600, \\ 4.1944\,10^{-4}\,T^{0.671118} & 600 \ge T, \end{cases}$$

$\sigma_{c,\mathrm{Ar}} = 0.0$, $\rho_{\mathrm{Ar}} = 3.73\,10^{-3}$, $\mu_{\mathrm{Ar}} = 1.0$, $z_{\mathrm{Ar}} = 3/2$, $R_{\mathrm{Ar}} = 2.081308\,10^{-2}$.

For graphite felt insulation, we have

$$\kappa_{\mathrm{Ins}}(T) = \begin{cases} 8.175\,10^{-2} + 2.485\,10^{-4}\,T & T \le 1473, \\ -1.1902\,10^2 + 0.346838\,T - 3.9971\,10^{-4}\,T^2 + 2.2830\,10^{-7}\,T^3 & \\ -6.46047\,10^{-11}\,T^4 + 7.2549\,10^{-15}\,T^5 & 1473 \le T \le 1873, \\ -0.7447 + 7.5\,10^{-4}\,T & 1873 \ge T, \end{cases}$$

$\epsilon_{\mathrm{Ins}} = 0.2$, $\sigma_{c,\mathrm{Ins}}(T) = 2.45\,10^2 + 9.82\,10^{-2}\,T$, $\rho_{\mathrm{Ins}} = 170.00$, $\mu_{\mathrm{Ins}} = 1.00$,
$c_{\mathrm{sp,Ins}} = 2100.00$.

For the graphite, we have
$\kappa_{\mathrm{Graphite}}(T) = 37.715\ \exp(-1.96\,10^{-4}\,T)$,

$$\epsilon_{\mathrm{Graphite}}(T) = \begin{cases} 0.67 & T \le 1200, \\ 3.752 - 7.436\,10^{-3}\,T + 6.4163\,10^{-6}\,T^2 & \\ -2.3366\,10^{-9}\,T^3 - 3.0833\,10^{-13}\,T^4 & 1200 \le T \le 2200, \\ 0.79 & 2200 \ge T, \end{cases}$$

$\sigma_{\mathrm{c,Graphite}} = 10^4$, $\rho_{\mathrm{Graphite}} = 1750.0$, $\mu_{\mathrm{Graphite}} = 1.0$,
$c_{\mathrm{sp,Graphite}}(T) = 1/(4.411\,10^2\,T^{-2.306} + 7.97\,10^{-4}\,T^{-0.0665})$.

For the SiC crystal, we have
$\kappa_{\mathrm{SiC\text{-}C}}(T) = \exp(9.892 + (2.498\,10^2)/T - 0.844\ \ln(T))$,
$\epsilon_{\mathrm{SiC\text{-}C}} = 0.85$, $\sigma_{\mathrm{c,SiC\text{-}C}} = 10^5$, $\rho_{\mathrm{SiC\text{-}C}} = 3140.0$, $\mu_{\mathrm{SiC\text{-}C}} = 1.0$,
$c_{\mathrm{sp,SiC\text{-}C}}(T) = 1/(3.91\,10^4\,T^{-3.173} + 1.835\,10^{-3}\,T^{-0.117})$.

For the SiC powder, we have
$\kappa_{\mathrm{SiC\text{-}P}}(T) = 1.452\,10^{-2} + 5.47\,10^{-12}\,T^3$,
$\epsilon_{\mathrm{SiC\text{-}P}} = 0.85$, $\sigma_{\mathrm{c,SiC\text{-}P}} = 100.0$, $\rho_{\mathrm{SiC\text{-}P}} = 1700.0$, $\mu_{\mathrm{SiC\text{-}P}} = 1.0$, $c_{\mathrm{sp,SiC\text{-}P}} = 1000.0$.

The functions are programmed in our flexible software package WIAS-HiTNIHS.

In the next section we discuss the microscopic model.

2.4. Coupling method for Macroscopic and Microscopic Models: Operator Splitting. Often simple coupling via the parameters, e.g. target-temperature, growth velocity of the bulk, is enough for the problem.

Here we propose a new idea of coupling the model equations together, one the one hand the heat equations and on the other hand the kinetic equations for molecules.

For a first idea, we deal with abstract operators, which include the heat- and the kinetics equations.

In the following algorithm, an iteration method is proposed, with fixed splitting discretization step-size τ. On a sufficient small time interval $[t^n, t^{n+1}]$, we solve the following sub-problems consecutively for $i = 0, 2, \ldots 2m$. (cf. [4] and [1].)

$$\frac{\partial c_i(t)}{\partial t} = Ac_i(t) \ + \ Bc_{i-1}(t), \text{ with } \ c_i(t^n) = c^n \tag{2.10}$$

$$i = 1, 2, \ldots, j \ , \tag{2.11}$$

$$\frac{\partial c_i(t)}{\partial t} = Ac_{i-1}(t) \ + \ Bc_i(t), \text{ with } \ c_{i+1}(t^n) = c^n \ , \tag{2.12}$$

$$i = j+1, j+2, \ldots, m \ , \tag{2.13}$$

where we assume the operator A has a large time scale (macroscopic model) and B has a small time scale (microscopic model). Further $c_0(t^n) = c^n$, $c_{-1} = 0$ and c^n are initialization and starting conditions.

In the following we give an overview to the accuracy of the method, which is given in the convergence and the rate of the convergence.

THEOREM 2.1. *Let us consider the abstract Cauchy problem in a Banach space* $\mathbf{X}$

$$\begin{aligned} \partial_t c(t) = Ac(t) + Bc(t), \quad 0 < t \leq T \\ c(0) = c_0 \end{aligned} \tag{2.14}$$

where $A, B, A + B : \mathbf{X} \to \mathbf{X}$ *are given linear operators being generators of the* C_0*-semigroup and* $c_0 \in \mathbf{X}$ *is a given element. Then the iteration process (2.10)–(2.12) is convergent. The rate of convergence is of higher order and given as* $\mathcal{O}(\tau_n^{2m})$*, where the iterations are* $i = 1, 3, \ldots, 2m + 1$.

The proof is given in [1].

In the next subsection we present the methods for the microscopic model.

3. Microscopic Model: Quantum Chemical Molecular Dynamics (QM/MD) of SiC Condensation (Methodology). The density-functional tight-binding (DFTB) method is employed as the quantum chemical potential in our molecular dynamics (MD) simulations, using atomic and diatomic parameters obtained from density functional theory, see [16]. DFTB is an approximate density functional theory method based on the tight binding approach, and utilizes an optimized minimal LCAO Slater-type all-valence basis set in combination with a two-center approximation for Hamiltonian matrix elements. Parameter sets for Si-Si and Si-C were taken from Ref.[19]. Energies and gradients are evaluated direct (on the fly) during the dynamic simulation. As in our previous simulations of carbon cap[17] and subsequent nanotube formation [18] on the C- and Si-faces of SiC(000-1) surfaces during sublimation evaporation, we have not included charge- or spin-polarization in the present work.

For time propagation we employed a velocity Verlet integrator with a time step of 1.209 fs (50 atomic units) and used a Nose-Hoover chain thermostat to generate a canonical ensemble for target temperature T_t. The thermostat was employed uniformly in the reaction system.

Regarding the atomistic structure of the employed surface model systems, we have chosen the C-face of the same square SiC(000-1) slab unit cell as in our previous study, [18] consisting of two SiC layers terminated by hydrogen atoms to mimic bulk effect in the direction away from the surface. Periodic boundary conditions were employed with a unit cell size of 1000 Å in the direction perpendicular to the surface

and 16.0 Å and 15.4 Å in the other two surface-directions to achieve two-dimensional slab periodicity. The geometry optimized structure of this surface model is shown in Figure 3.1.

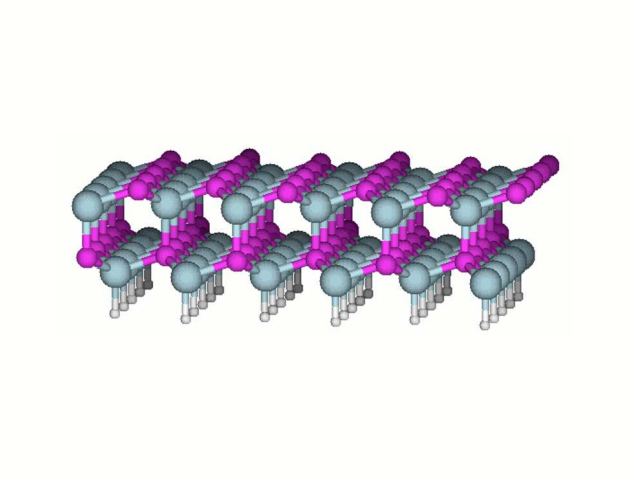

FIG. 3.1. *Optimized geometry as initial condition for the SiC surface.*

During MD simulations, the movements of hydrogen terminating atoms were frozen. Using such an approach, we have effectively introduced a steep temperature gradient from the deepest bulk-side SiC layer to the atoms lying above on the surface. The slab model was then annealed at T_t=2000 K for 1.20 ps, and 3 structures were selected as initial starting geometries at t=0.60 ps (trajectory A50), t=0.72 ps (trajectory A60), and t=0.86 ps (trajectory A80). In the vicinity of the surface, 10 SiC molecules were randomly distributed in the gas phase. Since these molecules are non-bonded to the surface, they are subsequently thermostated at T_t. Gas phase molecules approaching the surface will experience immediate cooling, which will drive the condensation process during these simulations.

In the next section, we present results of our numerical experiments.

4. Numerical experiments. We present in the following our macro- and microscopic simulations, where the microscopic simulations taken into account the target temperature of the macroscopic model.

4.1. Macroscopic Model: Simulation of the Temperature Field in the Apparatus. For the numerical results, we apply the parameter functions in Section 2.3. We consider the geometry shown in Fig. 2.1, using a constant total input power of 10 kW, cf. [13]. The numerical experiments are performed using the software WIAS-HiTNIHS, cf. [12], based on the software package *pdelib*, cf. [2], which uses the sparse matrix solver *PARDISO*, cf. [15]. We compute the coupled system consisting of the heat equations and Maxwell's equations. For the growth process, the temperature difference $T_{\rm ss} = T(r_{\rm source}, z_{\rm source}) - T(r_{\rm seed}, z_{\rm seed})$ (with the coordinates $(r_{\rm source}, z_{\rm source}) = (0, 0.143)$ and $(r_{\rm seed}, z_{\rm seed}) = (0, 0.158)$, corresponding to the points $T_{\rm source}$ and $T_{\rm seed}$ in Fig. 2.1) is crucial. On the other hand, in the physical growth experiments, usually only the temperatures $T(r_{\rm bottom}, z_{\rm bottom})$ and $T(r_{\rm top}, z_{\rm top})$ (with

the coordinates $(r_{\text{bottom}}, z_{\text{bottom}}) = (0, 0.028)$ and $(r_{\text{top}}, z_{\text{top}}) = (0, 0.173)$, corresponding to the points T_{bottom} and T_{top} in Fig. 2.1) are measurable and their difference $T_{\text{bt}} = T(r_{\text{bottom}}, z_{\text{bottom}}) - T(r_{\text{top}}, z_{\text{top}})$ is often used as an indicator for T_{ss}. In Fig. 4.1, we present the temperature differences T_{ss} and T_{bt}. As a result of our computations, the temperature difference T_{bt} can only restrictively be used as an indicator for the temperature difference T_{ss}, cf. the discussions in [5] and [9].

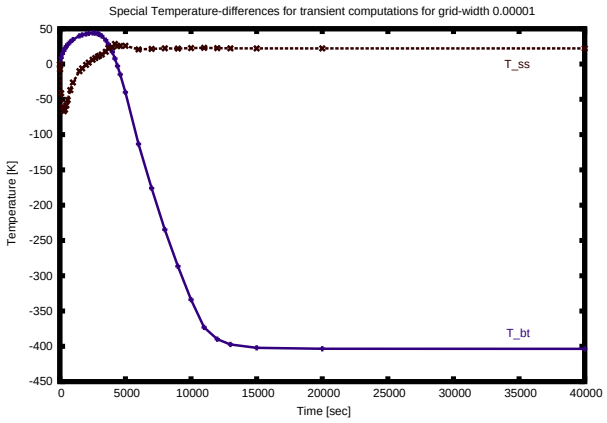

FIG. 4.1. *Transient results for the temperature differences T_{bt} and T_{ss}.*

The further computations are based on the stationary case, dealing with Equation (2.1) by discarding the terms with a time derivative. For this case, the results are virtually equal to the one in the transient case with $t > 15000$ sec. For the stationary results, we focus on the error analysis for the space dimension by applying the grid refinement. The solutions for the heat equation are computed at the points $T(r_{\text{bottom}}, z_{\text{bottom}})$ and $T(r_{\text{top}}, z_{\text{top}})$ for successive grids. For the error analysis, we apply the following error differences

$$\epsilon_{\text{abs}} = |\tilde{T}_{j+1}(r, z) - \tilde{T}_j(r, z)|, \tag{4.1}$$

where $\tilde{T}_j(r, z)$ and $\tilde{T}_{j+1}(r, z)$ are solutions evaluated at the point (r, z) which have been computed using the grids j and $j + 1$ respectively. The elements of the grid $j + 1$ are approximately $1/4$ of the elements of the grid j. The results are presented in Table 4.1.

Grid		Grid Point $(0, 0.028)$ (T_{bottom})		Grid Point $(0, 0.173)$ (T_{top})	
Level	Number of Nodes	Solution T [K]	Absolute Difference T [K]	Solution T [K]	Absolute Difference T [K]
0	1532	2408.11		2813.29	
1	23017	2409.78	1.67	2812.78	1.01
2	91290	2410.35	0.57	2811.79	0.49
3	364225	2410.46	0.11	2811.60	0.19

TABLE 4.1

Computations on different grids for the errors analysis with absolute differences, cf. equation (4.1).

The result of the refinement indicates the reduction of the absolute difference

as it is demanded for the convergence of the discretization method. The method is stabilized in the presented refinement by reducing the differences.

In Fig. 4.2, the temperature field is presented for the stationary case. The temperature increases from the bottom to the middle of the graphite pot, and decreases from the middle to the top of the graphite pot.

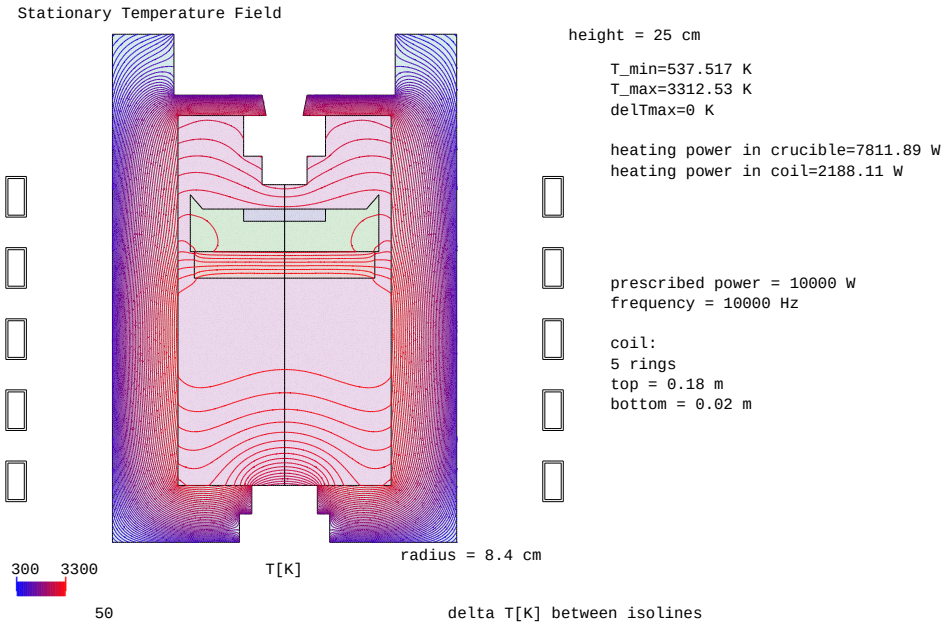

FIG. 4.2. *Temperature field for the apparatus simulated for the stationary case with* 23017 *nodes.*

4.2. Microscopic Model: Atomistic QM/MD simulations of SiC condensation on the C-face of Si(000-1). The total time of the three condensation simulations was 24.02 ps. This is admittedly a time too short for the study of crystal growth, which would ideally require annealing simulations on the order of several 100 nanoseconds, but this study is focusing on the initial stages of SiC aggregation and tries to identify key features in the condensation process. As such, this is at present rather a preliminary study exploring the applicability of QM/MD simulations for SiC crystal growth. We have first concentrated on the polar C-surface of SiC (0001) since it has a maximum of dangling bonds with highest reactivity. The Si-face and other, non-polar surfaces are much less reactive, see [20]. Since our seed crystal surface slab model contains only two SiC layers, we are also unable to address the issue of polymorphism at present.

T_t was chosen as 2000 K for all simulations, and representative snapshots from trajectory A50 are given in Figure 4.3. We find that under the present conditions with a relatively high density of SiC gas molecules, several of them attach very quickly to the surface (2 after 0.10 ps). Also, SiC molecules can react with themselves to form dimers, preferably with C-C bonds. Eventually, an average of 5.3 SiC molecules become attached to the surface in the three simulations, with the other molecules being lost to the vacuum layer.

Once attached, the Si atoms on the surface prove to be highly mobile, as their bond radius is larger than the case of carbon, and the binding energies are lower [17]. The carbon atoms on the surface tend to form C_2 units, and behave similar

to "wobbling C_2" entities that we had observed for high-temperature simulations of pure carbon, see [21]. It seems from our simulations at this stage that the system tries to reach an equilibrium with a constant number of C-C in the new layers, and that the Si atoms are more isolated, becoming occasionally attacked by a C_2 dimer. The surface itself retains the structure of alternating $Si-C$ units. Addition of more SiC molecules would be necessary to continue the study of layer buildup, and longer time for annealing.

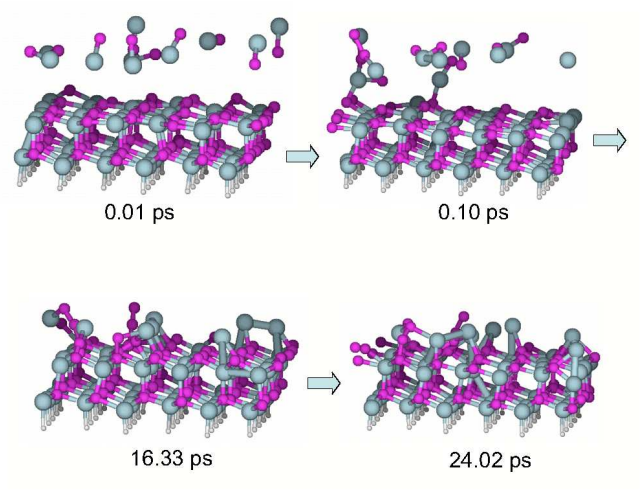

FIG. 4.3. *Simulation of the SiC surface* $T = 2000K$.

5. Summary. We have presented a model for the heat transport inside a technical apparatus for crystal growth of SiC single crystals. We introduce the heat equation and the radiation of the apparatus and the coupled situation of the different materials. The equations are discretized by the finite volume method and the complex material functions are embedded in this method. Transient and stationary results are presented leading to some information about the processes within the technical apparatus. We present numerical results for the stationary case to support the accuracy of our solutions. We also presented atomistic quantum chemical molecular dynamics (QM/MD) simulations based on the density-functional tight-binding (DFTB) method for initial reactions of gaseous SiC on the polar C-face of SiC(000-1). In our future work, we concentrate on further implementations and numerical methods for a crystal growth model and use kinetic data obtained from more accurate microscopic model simulations in the simulation of the heat transport.

REFERENCES

[1] I. Farago and J. Geiser. *Iterative Operator-Splitting methods for Linear Problems.* International Journal of Computational Science and Engineering, 3(4), 255-263, 2007.

[2] J. Fuhrmann, Th. Koprucki and H. Langmach. *pdelib : An open modular tool box for the numerical solution of partial differential equations. Design patterns.* In W. Hackbusch and G. Wittum;, editors, Proceeding of the 14th GAMM Seminar on Concepts of Numerical Software, January 23 - 25, 1998. Kiel, 2001.

[3] J. Geiser. *R^3T : Radioactive-Retardation-Reaction-Transport-Program for the Simulation of radioactive waste disposals.* Technical report, Institute for scientific computation, Texas A&M University, College Station, April 2004.

[4] J. Kanney, C. Miller and C. Kelley. *Convergence of iterative split-operator approaches for approximating nonlinear reactive transport problems.* Advances in Water Resources, 26, 247–261, 2003.

[5] O. Klein, P. Philip. *Transient temperature phenomena during sublimation growth of silicon carbide single crystals.* Journal of Crystal Growth, 249, 514-522, 2003.

[6] O. Klein and P. Philip. *Transient numerical investigation of induction heating during sublimation growth of silicon carbide single crystals.* J. Crystal Growth, 247, no. 1-2, 219–235, 2003.

[7] O. Klein and P. Philip. *Transient conductive-radiative heat transfer: Discrete existence and uniqueness for a finite volume scheme.* Preprint No. 871, Weierstrass-Institute for Applied Analysis and Stochastics, Berlin 2003.

[8] O. Klein and P. Philip. *Correct voltage distribution for axisymmetric sinusoidal modeling of induction heating with prescribed current, voltage, or power.* IEEE transactions on Magnetics, 38, no. 3, pp. 1519-1523, 2002.

[9] O. Klein, P. Philip and J. Sprekels. *Modeling and simulation of sublimation growth of SiC bulk single crystals.* Interfaces and Free Boundaries, 6, 295-314, 2004.

[10] St.G. Müller, R.C. Glass, H.M. Hobgood, V.F. Tsvetkov, M. Brady, D. Henshall, D. Malta, R. Singh, J. Palmour and C.H. Carter Jr. *Progress in the industrial production of SiC substrate for semiconductor devices.* Mater. Sci. Eng. ,B 80 , no. 1-3, 327–331, 2002.

[11] O. Nilsson, H. Mehling, R. Horn, J. Fricke, R. Hofmann, S.G. Müller, R. Eckstein, and D. Hofmann. *Determination of the thermal diffusivity and conductivity of monocrystalline silicon carbide (300-2300 K).* High Temp. - High Press., 29, no. 1, 73–80, 1997.

[12] P. Philip. *Transient Numerical Simulation of Sublimation Growth of SiC Bulk Single Crystal. Modeling, Finite Volume Method, Results.* Report No. 22, Weierstrass-Institute for Applied Analysis and Stochastics, Berlin, 2003.

[13] M. Pons, M. Anikin, K. Chourou, J. Dedulle, R. Madar, E. Blanquet, A. Pisch, C. Bernard, P. Grosse, C. Faure, G. Basset, and Y. Grange. *State of the art in the modeling of SiC sublimation growth.* Mater. Sci. Eng. B, **61**–**62**, 18–28, 1999.

[14] J. Rappaz and M. Swierkosz. *Modelling in numerical simulation of electromagnetic heating.* Modelling and optimization of distributed parameter systems, New-York. Chapmann & Hall, 313–320, 1996.

[15] O. Schenk, K. Gärtner. *Solving unsymmetric sparse systems of linear equations with PARDISO* J. Future Generation Computer Systems, **20**, no. 3, 475–487, 2004.

[16] D. Porezag, T. Frauenheim, T. Köhler, G. Seifert, and R. Kaschner. *Construction of tight-binding-like potentials on the basis of density-functional theory: Application to carbon* Phys. Rev. B **51**, 12947–12957, 1995.

[17] S. Irle, Z. Wang, G. Zheng, K. Morokuma, M. Kusunoki. *Theory and Experiment Agree: SWNT Caps Grow Catalyst-Free with Chirality Preference on a SiC Surface sublimation decomposition* J. Chem. Phys. **125**, 044702/1–044702/5, 2006.

[18] Z. Wang, S. Irle, G. Zheng, M. Kusunoki, K. Morokuma. *Carbon nanotubes grow on the C-Face of SiC (000-1) during sublimation decomposition: Quantum chemical molecular dynamics simulations* J. Phys. Chem. C **111**, 12960–12972, 2007.

[19] E. Rauls, Z. Hajnal, P. Deak, Th. Frauenheim. *Theoretical study of the nonpolar surfaces and their oxygen passivation in 4H- and 6H-SiC* Phys. Rev. B **64**, 245323/1–245323/7, 2001.

[20] J. Pollmann, P. Krüger, M. Sabisch. *Atomic and Electronic Structure of SiC Surfaces from ab-initio Calculations* Phys. Stat. Sol. B **202**, 421-445, 1997.

[21] S. Irle, G. Zheng, M. Elstner, K. Morokuma. *Formation of Fullerene Molecules from Carbon Nanotubes: A Quantum Chemical Molecular Dynamics Study* Nano Lett. **3**, 465-470, 2003.